ACS EARTH AND SPACE CHEMISTRY

http://pubs.acs.org/journal/aesccq

Article

Photodegradation of Secondary Organic Aerosols by Long-Term Exposure to Solar Actinic Radiation

Vahe J. Baboomian, Yiran Gu, and Sergey A. Nizkorodov*

Cite This: *ACS Earth Space Chem.* 2020, 4, 1078−1089

Read Online

ACCESS | Metrics & More | Article Recommendations | Supporting Information

ABSTRACT: Sunlight-driven chemical transformations of secondary organic aerosol (SOA) are important for understanding the climate- and health-relevant properties of atmospheric particulate matter, but these photochemical processes are not well understood. We measured the photodegradation rates of SOA by observing condensed-phase photochemical processes over many days of UV exposure. The experiments relied on a quartz crystal microbalance to quantify the mass loss rate from SOA materials prepared by ozonolysis of D-limonene and α-pinene and photo-oxidation of toluene under either high or low NO_x conditions. We observed that 254 nm irradiation degraded SOA almost entirely after 24 h. The mass loss rates were higher for toluene-derived SOA, which absorbs strongly at 254 nm. Irradiation at 305 nm, which is more relevant for the troposphere, resulted in larger mass loss rates from SOA generated from α-pinene and D-limonene, even though toluene-derived SOA had a higher absorption coefficient. In all 305 nm irradiation experiments, the initial mass loss rate was high (corresponding to 1−5% fractional mass loss per hour), but it slowed down after 24 h of irradiation, with a photorecalcitrant fraction of SOA degrading much slower (<1% fractional mass loss per hour). The mass loss rates were observed to increase at a higher relative humidity because volatile photoproducts could diffuse out of SOA faster. Long-term changes in the chemical composition of limonene ozonolysis SOA were examined using high-resolution electrospray ionization mass spectrometry and revealed a more complex mixture of species after photodegradation compared to the initial SOA. The compounds in the photodegraded sample had on average lower molecular weights, lower H/C ratios, and higher O/C ratios compared to the compounds in the un-photolyzed sample. These experiments confirm that condensed-phase photochemistry is an important aging mechanism for SOA during long-range transport.

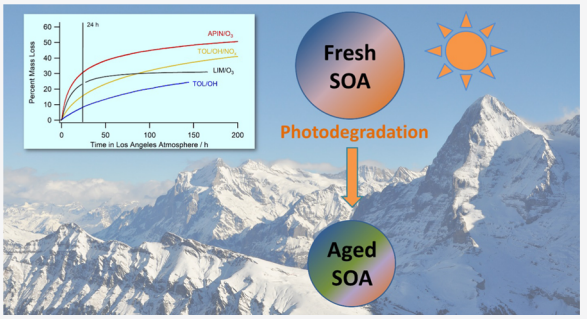

KEYWORDS: *condensed-phase photochemistry, photolysis, atmospheric organic aerosol, chemical aging, particle mass loss*

INTRODUCTION

Secondary organic aerosol (SOA) represents the dominant fraction of atmospheric particulate matter and is formed in the atmosphere by the condensation of oxidation products of volatile organic compounds (VOCs). VOCs are emitted from both biogenic sources, such as vegetation, and anthropogenic sources, such as incomplete fossil fuel combustion and industrial processes.[1] Common biogenic VOCs include isoprene, α-pinene, D-limonene, and other terpenes, while common anthropogenic VOCs include aromatic hydrocarbons and saturated aliphatic hydrocarbons found in fossil fuel. Once emitted, VOCs undergo oxidation to form lower-volatility oxygenated VOCs, which can contribute to new particle formation or partition into pre-existing particulate matter.[2−4] Once formed, SOA travels through the atmosphere and undergoes various chemical aging reactions that change its physicochemical properties. The current understanding of SOA aging processes is limited, and this uncertainty contributes to the challenges of quantifying the environmental impacts of SOA.[5,6]

The production, aging, and loss of SOA sensitively depend on environmental conditions such as humidity, temperature, trace gas concentrations, and solar irradiance. Aging is especially challenging to integrate into models due to the multiple mechanisms by which it can occur. Aging processes include heterogeneous oxidation of particles by OH, reactive and nonreactive uptake of semivolatile species, and various condensed-phase reactions, such as direct photolysis, photosensitized reactions, reactions involving free radicals produced inside particles, and nonradical processes, such as hydrolysis.[7−9] Photodegradation reactions tend to fragment the SOA organics into smaller, more volatile compounds, which can evaporate into the gas phase leading to SOA mass loss.[10−14]

Received: April 7, 2020
Revised: May 26, 2020
Accepted: June 1, 2020
Published: June 1, 2020

These higher-volatility species have been shown to include CO, CO_2, methane, acetic acid, formic acid, acetone, acetaldehyde, and other small organic molecules.[12,15,16] These photodegradation processes affect the Earth's climate because they reduce the mass concentration and particle diameter, making SOA scatter sunlight less efficiently.[17]

Compounds containing carbonyl and peroxide functional groups are examples of photochemically active species responsible for the SOA mass loss under tropospheric sunlight ($\lambda > 295$ nm).[16,18,19] The C−C(O) bond in carbonyls can be broken by Norrish type-I and Norrish type-II photocleavage processes to form smaller products.[10,16,20] Peroxides break at the weak O−O bond, forming two O-centered radicals, which undergo secondary processes on a picosecond time scale.[21] However, not all photochemical processes result in fragmentation. Secondary reactions of free radicals in the SOA particles can also lead to oligomerization products that increase the carbon number of SOA species and lead to a lower-volatility SOA mixture.[20]

Previous experimental studies have shown that photodegradation of the condensed-phase material in SOA can occur on atmospherically relevant time scales.[7,10,11,13] A modeling study has predicted that SOA mass would decrease by 40−60% after 10 days of atmospheric aging if condensed-phase photochemical processes are permitted and proceeded at the same rate as in the gaseous phase.[22] A recent combined experimental and modeling study also predicted about 50% reduction in biogenic SOA in the Amazon region due to SOA photodegradation.[23] Such photodegradation processes are particularly important for free tropospheric aerosols, which can have mean residence times four times as large compared to those trapped by the boundary layer,[24] and have more time to contribute to cloud formation and the Earth's energy budget.[25−27] Obtaining a better understanding of long-term photochemical aging processes is necessary to understand the fate of SOA and can potentially improve model-measurement discrepancies.[25,28]

Insights into SOA aging by condensed-phase photochemistry have been gained via laboratory experiments where SOA was aged in batch chambers[13,14,23,29] or flow tubes,[10] immobilized on substrates,[20,30−33] or extracted into solution.[33−38] Aerosols have lifetimes of ∼1 week in the atmosphere, but typical chamber studies are conducted from a few hours to 1−2 days at the longest.[13,23,29] Long-term aging is usually investigated by selecting the experimental conditions to allow laboratory time scales to reach atmospheric values. In studies of aging driven by heterogeneous OH oxidation, unrealistically high OH radical concentrations have been used to reach equivalent atmospheric exposure times of ∼1−2 weeks in a matter of minutes in an oxidation flow reactor.[39] For photochemistry, a related approach would be equivalent to increasing the intensity of UV radiation way above the level normally found in the atmosphere.[10] In either case, the results are then extrapolated to atmospheric conditions assuming that the processes scale linearly with OH concentration and/or UV radiation flux and wavelength dependence. This method may not be entirely accurate though, as the mechanism of aging processes in SOA can change under elevated oxidant concentrations and solar fluxes.[20] Indeed, recent studies have begun investigating condensed-phase long-term aging and have found appreciable differences in the aging mechanisms and changes in composition compared to short-term aging studies.[20,29] For example, Walhout et al. irradiated α-pinene ozonolysis SOA collected on Teflon filters for 4 days and found photofragmentation reactions to be the dominant process in the first 2 days of aging, after which oligomerization reactions between photoproducts become more important.[20] Further experiments are needed over long laboratory time scales with more typical levels of oxidants and UV radiation to better understand the rates of aging processes occurring in the atmosphere.

Until recently, observations of aging driven by condensed-phase photochemistry in SOA have been largely exploratory and at best gave only a rough estimate of the mass loss rate. More recent studies have been able to directly measure the rate of photodegradation of the SOA material, but only for a limited number of SOA types and under short time scales.[12,23] The humidity dependence of SOA photodegradation rates also remains an open question because most of the previous studies, with a few exceptions,[13,23,32] relied on dry conditions. The goal of this work was to extend the study done by Malecha et al.[12] by quantifying the long-term photodegradation of SOA derived from representative biogenic and anthropogenic VOCs and investigate the effects of humidity on the mass loss rate. This was accomplished using a quartz crystal microbalance (QCM) to directly track the changes in SOA mass due to photodegradation as a function of time. Our results support the conclusion that condensed-phase photochemistry can lead to large mass loss from SOA particles over long periods of solar radiation exposure, thus counteracting aerosol particle growth due to gas-to-particle partitioning.

MATERIALS AND METHODS

SOA Samples. Four different types of SOA were investigated for this study: α-pinene ozonolysis (APIN/O_3), D-limonene ozonolysis (LIM/O_3), toluene low-NO_x photo-oxidation (TOL/OH), and toluene high NO_x photo-oxidation (TOL/OH/NO_x). The ozonolysis and TOL/OH samples were prepared using two different flow reactors, while the TOL/OH/NO_x samples were prepared in a photo-oxidation chamber operated in a batch mode. A summary of all of the samples made in this study can be found in Table S1.

The O_3-initiated SOA was formed in an ∼20 L flow tube reactor where liquid pure APIN or LIM was injected by a syringe pump at 25 μL/h into 5 SLM flow of zero air. A 1 SLM flow of oxygen was sent through an ozone generator and an ozone photometric detector. The O_3- and VOC-containing flows were mixed at the entrance of the flow cell to achieve starting mixing ratios of 14 and 10 ppm, respectively. The flow tube residence time was ∼3.5 min and was sufficient to form SOA. A charcoal denuder was used at the flow tube exit to scrub excess O_3 before collecting SOA. For the TOL/OH sample, a different flow reactor was used as described in Veghte et al.[40] Briefly, this oxidation flow reactor involved an 8 L quartz reaction vessel surrounded by two 254 nm UV lamps inside a Rayonet RPR100 photochemical reactor. The pure VOC was injected using a syringe pump into zero air flowing into the reaction vessel, where it mixed with O_3. The UV lamps converted O_3 to OH by reacting with H_2O, OH reacted with toluene, and the SOA was collected from the exit tube.

The aerosol smog chamber used for making TOL/OH/NO_x SOA was a 5 m^3 Teflon bag surrounded by a bank of 42 UV-B lights. The chamber was equipped with a scanning mobility particle sizer (SMPS) to monitor particle concentrations and a proton-transfer-reaction mass spectrometer (PTR-MS) to monitor VOC concentrations. The SOA was prepared similar

https://dx.doi.org/10.1021/acsearthspacechem.0c00088
ACS Earth Space Chem. 2020, 4, 1078−1089

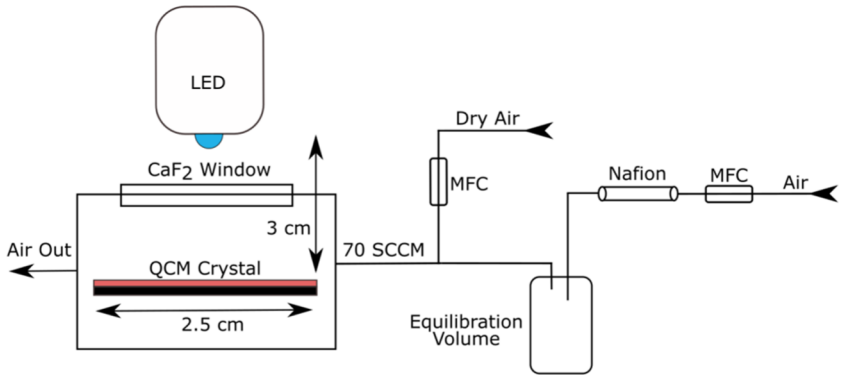

Figure 1. SOA photodegradation setup. The QCM crystal with SOA is placed into the QCM oscillator. A 305 nm LED, 405 nm LED, or 254 nm pen-ray lamp is mounted above the sample and irradiates the SOA continuously. The photoproducts are purged out of the QCM setup through an exit port by a slow flow of zero air. A humidifier is used to control the relative humidity (RH) of the air flow.

to previous experiments on TOL/OH/NO_x SOA.[41] The starting VOC, H_2O_2, and NO_x mixing ratios were 1, 2, and 0.5 ppm, respectively. After the VOC was injected and its concentration stabilized, H_2O_2 and NO_2 were injected in the chamber, and finally, panels of UV-B lights were turned on, resulting in a steady-state OH concentration of $\sim 10^6$ molecules cm^{-3}. After 4 h of photo-oxidation of the VOC by OH, the SOA was collected. It is important to note that the VOC concentrations used in this study are much higher than those found in the atmosphere. These conditions can favor certain reaction pathways that can lead to differences in the SOA composition (which in turn may affect their photodegradation processes). For example, the higher mass loadings used in this study can increase the particle-phase partitioning of volatile carbonyl-containing compounds, which may lead to an overestimate of the photodegradation extent in the atmosphere.[2]

In all cases, the SOA was collected onto Stage 7 (0.32−0.56 μm particle size) of a micro-orifice uniform deposit impactor (MOUDI; MSP Corp. model 110-R) for 1−4 h with custom adapters to accommodate a 2.54 cm diameter chrome/gold QCM crystal as the substrate. The MOUDI was used to ensure a more uniform deposition of particles on the substrate, and Stage 7 was used since it provided the largest amount of SOA mass to be collected. The resulting SOA material was preconditioned by keeping the QCM crystal under a flow of clean, dry air overnight at 40 °C to remove the more volatile compounds and allow the particles to better adhere to the QCM substrate and merge into a more continuous film. During this preconditioning step, the more labile SOA compounds, such as peroxide, likely decomposed, so these measurements probe the behavior of more thermally stable SOA compounds.[42,43] The masses collected ranged from 0.05 to 3.4 mg (Table S1), as determined by weighing the crystal before and after the collection (and after preconditioning) with a Sartorius ME5-F microbalance (1 μg precision). Assuming an SOA material density of 1.2 g cm^{-3} and 1 mg of SOA deposited, we estimate the effective SOA material thickness to be 1.6 μm on the 5 cm^2 QCM crystal.

SOA Photodegradation Setup. A commercial QCM was modified to include a sealed space above the QCM crystal with a CaF_2 window on top to allow the sample to be irradiated (Figure 1).[12] A flow of 70 SCCM of clean air was passed over the sample to drive off the photoproducts. To investigate the effects of humidity on photodegradation rates, the humidity of the air flow above the sample was controlled by mixing dry air with humid air that had passed through a Nafion single-channel humidifier (PermaPure). Two light sources were used in this study to drive photodegradation: a light-emitting diode (LED) centered at 305 nm (Thorlabs Inc., model M300L4) and a mercury pen-ray lamp centered at 254 nm (Spectronics Corp. model Spectroline 11SC-1). The 305 nm LED was used to represent tropospheric UV radiation (below ozone layer), while a 254 nm lamp was used in proof-of-concept experiments. In addition, an LED centered at 405 nm (Thorlabs Inc., M405L4) was used in control experiments, where samples were irradiated but not expected to undergo photodegradation.[12] Using selected wavelengths of radiation as opposed to a full solar spectrum made it possible to investigate the wavelength dependence of the photodegradation. It also avoided unnecessary heating of the sample with visible and near-infrared radiation coming from broadband radiation sources, such as arc lamps. The incident power of each lamp was measured using a Coherent PS19Q power meter in the same geometry that was experienced by the QCM crystal. The resulting powers were 2.6 mW for the 305 nm LED and 3.7 mW for the 254 nm lamp. Previous experiments have shown that these power meter measurements agree reasonably well with actinometry experiments.[11,44]

Exposure to UV radiation reduces the SOA mass on the crystal (due to the evaporation of volatile photoproducts) and increases the crystal oscillation frequency. To convert the observed change in frequency into change in SOA mass, a modified version of Sauerbrey's equation was used[45]

$$\frac{dm}{dt} = -\frac{1}{C_f}\frac{df}{dt} \quad (1)$$

where $\frac{df}{dt}$ is the rate of frequency change during irradiation (Hz/h), C_f is the sensitivity factor (Hz/μg), and $\frac{dm}{dt}$ is the mass change rate (μg/h). The C_f was determined empirically through calibration experiments as performed in previous studies.[12,46] C_f was calculated by measuring the frequency of the clean crystal, collecting SOA on the crystal, weighing the amount of mass impacted onto the crystal (Δm), and noting the frequency change (Δf) experienced by the QCM. The sensitivity factor was then calculated through the integrated form of eq 1.

$$C_f = -\frac{\Delta f}{\Delta m} \quad (2)$$

https://dx.doi.org/10.1021/acsearthspacechem.0c00088
ACS Earth Space Chem. 2020, 4, 1078−1089

The resulting sensitivity factors for different SOA samples are listed in Table S1. They ranged from about 10 to 24 Hz/μg. With the 0.1 Hz precision of the instrument, this translates into an effective sensitivity of 4−10 ng for the SOA mass change on the crystal.

Characterization of SOA. A direct infusion electrospray ionization mass spectrometer (ESI-MS) was used to assess the extent of composition changes of LIM/O_3 SOA due to long-term photodegradation. The instrument was a Thermo Q Exactive Plus, operated at a mass resolving power of 1.4×10^5. The ESI-MS was operated in a positive ion mode at a spray voltage of 3.5 kV, and the analyte was extracted off the QCM crystal using a 1:1 solution of acetonitrile/water with an analyte mass concentration of 0.8 mg/mL. Peak positions and relative abundances were extracted from the raw data using Decon2LS (https://omics.pnl.gov/software/decontools-decon2ls). The peaks were assigned with 0.001 m/z accuracy with formulas of $[C_cH_hO_o + Na]^+$ (formation of sodium adducts was the dominant ionization mechanism; no protonated ions $[C_cH_hO_o + H]^+$ were detected). The mass spectra below are plotted as a function of the molecular weight of the unionized compounds $C_cH_hO_o$.

RESULTS AND DISCUSSION

Analysis of Sample Measurements. Figure 2a shows the observed QCM frequency change in a typical experiment. The frequency of the clean crystal is shown as the green line, and it was of the order of 5.010 MHz in this particular case. With LIM/O_3 SOA on the crystal surface, the frequency decreased to ∼4.994 MHz. Without irradiation under dry conditions, the frequency changed very slowly due to slow evaporation of SOA compounds from the substrate; an example of dark control measurements can be found in Figure S1. The frequency began to increase once the 305 nm LED was turned on at the 0 h mark due to the loss of the volatile photoproducts. The frequency increase to the maximum value was not instantaneous as it takes time for the photoproducts to diffuse through and evaporate from the SOA matrix.[32] After the frequency began to stabilize, i.e., photodegradation slowed down, the LED was turned off (around 118 h in this example). We observed that turning off the LED slowed down the frequency change, suggesting that photodegradation was still faster than spontaneous evaporation.

Taking the derivative of the frequency curve and using eq 1 yielded the mass loss rate of the SOA (Figure 2b). A boxcar smoothing algorithm with a 10 min rolling averaging window was applied to remove the measurement noise caused by the clean air generator periodic purges. The smoothing did not distort the time dependence of the curves shown in Figure 2.

Plotting the mass loss as a percent mass loss (Figure 2c) shows the LIM/O_3 degrading until ∼30% of the initial mass is lost and stagnates afterward. This is particularly important, as it confirms that a photorecalcitrant (i.e., non-photodegradable) fraction of SOA remains after the more photolabile compounds are photodegraded.[20,29] The photorecalcitrant fraction is thought to consist of photochemically inactive SOA compounds left behind after photolabile carbonyl and peroxide compounds have undergone photodegradation.[29] Due to the photorecalcitrant SOA remaining on the crystal, the crystal frequency never recovered to its initial frequency (green line in Figure 2a). The overall accuracy of the mass loss rates was quantified by integrating the mass loss rates over the irradiation period to obtain the total mass lost. This value was

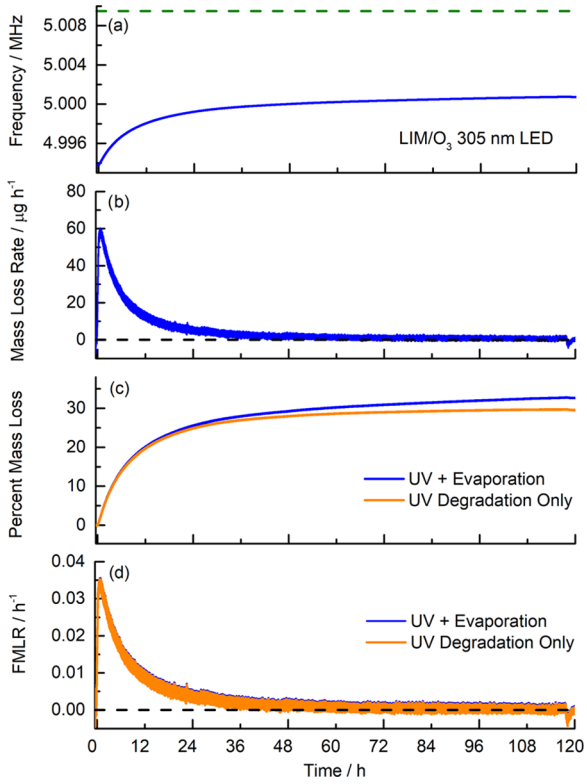

Figure 2. (a) Typical QCM experiment where the clean crystal frequency (green line) decreases once SOA has been impacted onto it. The LED was turned on at the 0 h mark, and the frequency began to increase due to the evaporation of photoproducts. After ∼120 h, the LED was turned off. (b) Mass loss rate profile of the LIM/O_3 sample. The black dashed line shows the zero point. (c) Percent mass loss of the same sample. (d) Fractional mass loss rate of the sample, where 0.035 h^{-1} corresponds to 3.5% mass loss per hour. The blue curves correspond to mass loss due to evaporation and UV degradation, while the orange curves correspond to mass loss from UV degradation alone.

compared to the mass lost by directly weighing the crystal before and after irradiation using the Sartorius ME5-F microbalance. The average percent deviation between QCM measurements and direct weighing was 8%, representing a reasonable accuracy.

Since the mass loss rate scaled linearly with the amount of SOA deposited on the crystal (Figure S2), the mass loss rates were normalized to the SOA mass remaining on the crystal to calculate the fractional mass loss rate (FMLR) (i.e., 0.035 h^{-1} at the peak of Figure 2d corresponds to 3.5% mass lost per hour). The FMLR curve (Figure 2d) has a similar shape to the mass loss rate (Figure 2b), but it decays to zero slower because the SOA mass on the crystal decreases with irradiation time. FMLR is a more useful metric to incorporate into models since it can be treated as a rate constant (with the caveat that it is not actually constant).

Control experiments were conducted (Figure S1), and the results showed that mass loss due to spontaneous evaporation (no UV irradiation) played a relatively minor role in comparison to photochemically driven mass loss. A control experiment was also conducted using a 405 nm LED to reproduce any thermal evaporation due to possible heating of the QCM crystal by the LED operation. The 405 nm LED was configured to the same power output as the 305 nm LED but was not expected to produce significant photodegradation.[12] In

https://dx.doi.org/10.1021/acsearthspacechem.0c00088
ACS Earth Space Chem. 2020, 4, 1078−1089

agreement with this expectation, the 405 nm LED produced the same mass loss rate as the evaporation in darkness. Thus, we can conclude that although spontaneous evaporation did occur in this experiment, its rate was small compared to the effect due to photodegradation. Furthermore, the effects of heating the QCM crystal by the LED were also unimportant. Although mass loss due to evaporation was found to be small compared to photodegradation, the mass loss was corrected to remove the effects of evaporation (Figure 4c) and further reveals the stagnation in photodegradation and the presence of a photorecalcitrant fraction. Removing the influence of evaporation from the FMLR (Figure 4d) resulted in a nearly identical mass loss profile. The evaporation correction method is discussed in more detail in the Supporting Information (SI).

Photodegradation at 254 nm. As mentioned in the experimental section, two different light sources were used to examine SOA photodegradation. Figure 3 shows the results of

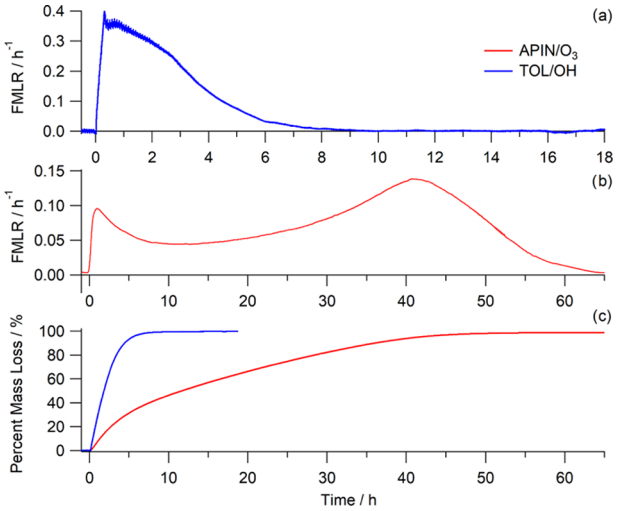

Figure 3. FMLR observed during 254 nm irradiation of (a) TOL/OH and (b) APIN/O_3SOA leads to nearly 100% of the SOA being degraded with no photorecalcitrant fraction remaining (c). The UV lamp was turned on at the 0 h mark.

irradiating APIN/O_3 and TOL/OH SOA with 254 nm radiation, which represents an extreme case and serves as a proof of concept of the experimental technique before investigating more subtle processes under tropospheric wavelengths. The TOL/OH sample exhibited a higher maximum FMLR and reached a degradation plateau faster than the APIN/O_3 sample. This is likely due to TOL/OH SOA having a much higher absorption coefficient than APIN/O_3 SOA.[47] In both samples, under 254 nm irradiation, nearly 100% of the mass was degraded. The APIN/O_3 sample exhibited a complex time dependence of FMLR, with an initial maximum at early times and a secondary maximum at later times (~40 h). This could suggest two fractions of SOA mass, one that is initially present and highly photodegradable and another that is slowly produced by secondary reactions of the initial photoproducts. Our results agree with the previous 254 nm photodegradation experiments on APIN/O_3 SOA,[12] which also observed rapid mass loss of SOA during irradiation. These experiments prove that organic aerosols are capable of being fully degraded under harsh UV radiation and show that we are able to accurately measure the mass loss rates of the process.

Photodegradation at 305 nm. The majority of our experiments relied on the 305 nm irradiation, which is more relevant for the lower atmosphere. Figure 4 summarizes the

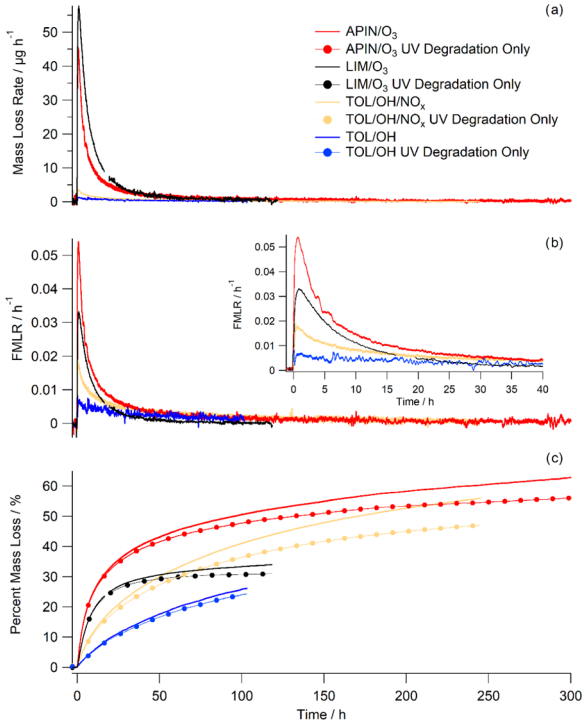

Figure 4. Mass loss rate (a), FMLR (b), and percent mass loss (c) observed during 305 nm irradiation of various SOA types. A photorecalcitrant fraction is observed in all samples, with APIN/O_3 SOA only degrading to ~60% after 300 h of irradiation. In panel (d), the dotted lines represent percent mass loss due to photodegradation only, after correcting for the dark evaporation (the equations used for the correction are given in the SI section).

results for four different types of SOA. The LIM/O_3 experiments were repeated in triplicate to check for reproducibility and showed good quantitative agreement in the measured FMLR values. The average of the three LIM/O_3 trials is shown in Figure 4, and the individual LIM/O_3 data are shown in Figure S3. There is a gap in the LIM/O_3 average trace due to QCM signal disconnection for a brief period in one of the runs.

After normalizing by mass loading and correcting for the effects of dark evaporation (Figure 4b), APIN/O_3 SOA showed the fastest photodegradation, followed by LIM/O_3 and TOL/OH/NO_x, and TOL/OH had the slowest rate. Interestingly, at 305 nm, the FMLR of APIN/O_3 SOA is larger than that for TOL/OH SOA, but the opposite order applies at 254 nm (Figure 3). This demonstrates strong dependence of these processes on the types of electronic transitions accessible at the two wavelengths, specifically n → π^* transitions at 305 nm vs $\pi \rightarrow \pi^*$ transition at 254 nm. The TOL/OH/NO_x sample showed a maximum FMLR ~2.5 times larger than the TOL/OH sample. This can be explained by TOL/OH/NO_x SOA absorbing more strongly than TOL/OH SOA due to the incorporation of nitrogen-containing organics.[48] In fact, the mass-normalized absorption coefficient at 305 nm of similarly prepared TOL/OH/NO_x SOA has been shown to be ~2.8 times higher than that for TOL/OH SOA.[47]

https://dx.doi.org/10.1021/acsearthspacechem.0c00088
ACS Earth Space Chem. 2020, 4, 1078−1089

The percent mass loss (from UV degradation alone and from the combination of evaporation and UV degradation) shown in Figure 4c is significant, with APIN/O_3 showing the largest percent of mass loss (~50% after 100 h) and TOL/OH showing the smallest (~20% after 100 h). After the initial rapid photodegradation, it slows down considerably for APIN/O_3 and LIM/O_3 even though the organic material still remains on the QCM crystal, signifying the formation of a more stable photorecalcitrant fraction. Previous studies have also noted a photorecalcitrant fraction after 40 h of irradiation of APIN/O_3 in a smog chamber and attributed this fraction to molecules that do not contain photochemically active groups, such as carbonyl and peroxide groups.[29] The formation of a photorecalcitrant fraction is less obvious in TOL/OH and TOL/OH/NO_x SOA, but their photodegradation also slows down with irradiation time. These measurements clearly demonstrate that the kinetics of SOA photodegradation cannot be modeled as a simple first-order process; at least two rate constants are needed to parameterize the mass loss rate in models.

While the number of SOA types investigated in this study is limited due to the long time required for these experiments, the data suggest that the biogenic SOA degrades more readily than SOA from aromatic precursors. The differences in FMLR are due to a combination of possible effects. One effect is that α-pinene and D-limonene ozonolysis products include more carbonyl and peroxide groups (which are expected to undergo efficient photofragmentation)[10,16,20,29] than the oxidation products produced from toluene photo-oxidation.[49−51] Experiments and theoretical calculations show that photolysis of carbonyls and peroxides remains efficient in the condensed phase, producing products with high quantum yields on picosecond time scales following the excitation.[21,52−54] Another effect is that the TOL/OH/NO_x SOA compounds may be more efficiently disposing of the electronic excitation energy by internal energy relaxation without breaking up into smaller products. TOL/OH/NO_x SOA components include aromatic species, such as nitrophenols, which have photolysis quantum yields approaching unity in the gaseous phase but only ~10^{-4}−10^{-5} in the condensed phase.[55,56] The excitation of nitrophenol clusters has been shown to result in fast internal conversion mediated by intramolecular hydrogen bonding.[57] These studies suggest that the SOA components may channel most of the excitation energy into heat, thus slowing the photodegradation and resulting in a low FMLR despite a high absorption coefficient. Guaiacol high NO_x SOA was also found to photodegrade slowly in previous experiments, and it was also attributed to the rapid internal energy relaxation in aromatic compounds.[12]

These results also indicate that the photodegradation is a dynamic process, which starts at a high rate, slows down, and eventually stops (Figure 4). Therefore, treating the initial photodegradation rates (e.g., rates determined by Malecha et al.)[12] as constant will lead to an overestimation of the effect of condensed-phase photochemistry on SOA mass concentration. A more reasonable representation is a biexponential decay of the SOA mass concentration as proposed by O'Brien et al.[29]

Effect on the Chemical Composition. High-resolution ESI(+) mass spectrometry was used to study the difference between the chemical composition of fresh SOA and the photorecalcitrant fraction in 305 nm experiments with LIM/O_3 SOA. Figure 5 shows a mass spectrum of both the nonirradiated (using the same collection and annealing method) and photorecalcitrant fraction of LIM/O_3 SOA.

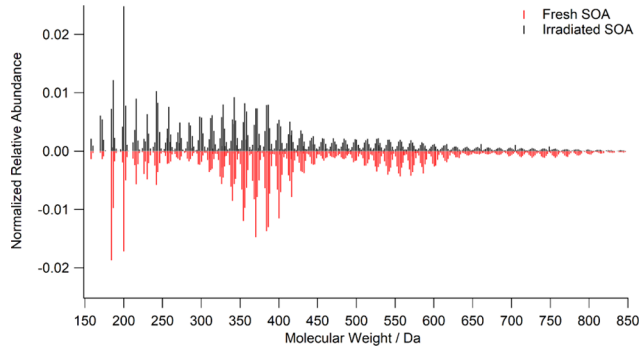

Figure 5. High-resolution ESI(+) mass spectra of irradiated (black) and fresh (red) LIM/O_3 SOA. The peaks are normalized to the combined peak abundance. The fresh data are inverted for the ease of comparison. While the fresh SOA has clearly separated monomer, dimer, and trimer regions, this distinction becomes less obvious in the irradiated SOA due to a combination of fragmentation, functionalization, and radical recombination reactions in SOA.

The signals were normalized to the total peak abundance. It is important to note that this analysis only probed molecular formulas. Thus, some of the newly formed products may have the same formula as the fresh sample but different chemical structures (for example, cis-pinonic acid is known to photoisomerize into its structural isomer limononic acid).[52] Also, while the effect of evaporation on the differences in mass spectra is expected to be small compared to the effects of photodegradation, some of the minor differences in the mass spectra are due to evaporation. The photorecalcitrant fraction showed a more complex mixture of compounds with less well-defined transitions between the monomer, dimer, and trimer regions. The fresh SOA sample contained 1010 compounds, while the photorecalcitrant fraction contained 1434 compounds, of which 495 were unique to the recalcitrant fraction. Photolysis of the initial SOA molecules splits them into smaller fragments and increases the degree of oxidation. However, this process can be partly counteracted by free-radical (RO_2) cross-reactions within the SOA matrix producing new oligomers.

To help compare fresh and irradiated LIM/O_3 SOA, the observed compounds were separated into three groups: (1) compounds that increased in normalized peak abundance by at least an order of magnitude compared to the fresh sample; (2) compounds that experienced a change in the normalized peak abundance by less than an order of magnitude; and (3) compounds that disappeared after irradiation. Compounds in groups 1 and 2 represent the photorecalcitrant fraction remaining in the irradiated LIM/O_3 SOA, while compounds in group 3 are photolabile. The O/C and H/C ratios of the compounds in each of the groups are compared in Figure 6a, and double bond equivalent (DBE) values are compared in Figure 6b. The abundance weighted average O/C, H/C, DBE, and number of C atoms for each of the groups, as well as for all of the observed peaks in the fresh SOA and irradiated samples are listed in Table 1. The overall trend shows larger O/C and smaller H/C ratios in molecules that are formed due to irradiation and contribute to the photorecalcitrant fraction (i.e., groups 1 and 2). Compounds in group 3 tend to have higher C-numbers consistent with the expectation that larger molecules have a higher probability of photodegradation. This is also seen in Table 2, with the most prominent compounds in group 3 containing higher C-numbers. Furthermore, photolabile group 3 compounds tend to have smaller DBE/C ratios,

https://dx.doi.org/10.1021/acsearthspacechem.0c00088
ACS Earth Space Chem. 2020, 4, 1078−1089

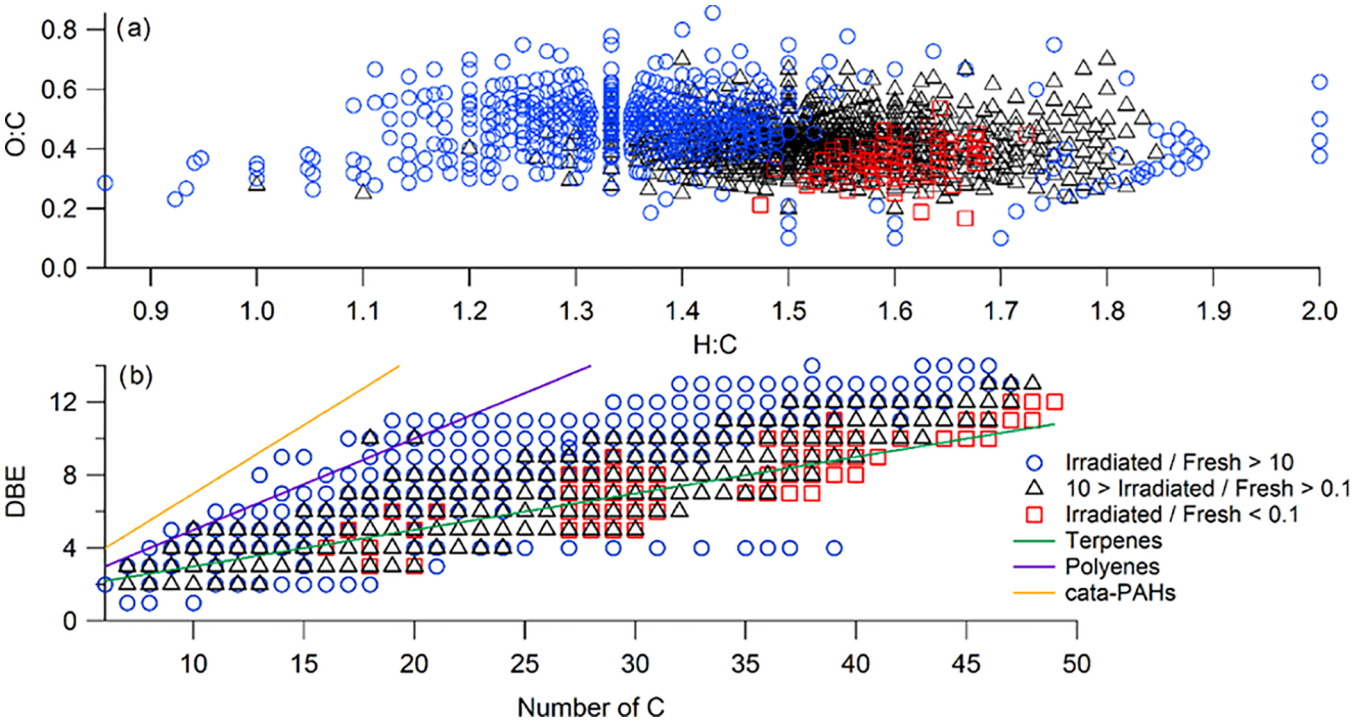

Figure 6. (a) O/C and H/C of LIM/O_3 SOA molecular species observed by ESI-MS. Please note the atypical Van Krevelen diagram, with the interchanged traditional axes. (b) Double bond equivalent (DBE) of the same compounds plotted as a function of the carbon number. In both panels, the blue circles correspond to molecules with a normalized peak abundance that increased by over an order of magnitude after long-term irradiation. The black triangles correspond to molecules whose normalized peak abundance changed by less than an order of magnitude, while the red squares correspond to molecules that disappeared after irradiation. The green, purple, and orange lines correspond to the expected DBE vs C dependence for terpene, polyene, and cata-PAH compounds, respectively. Photorecalcitrant molecules (blue circles and black triangles) tend to have a lower H/C ratio, higher O/C ratio, and increased DBE compared to photolabile compounds (red squares).

Table 1. Peak Abundance Weighted Average Composition Characteristics of LIM/O_3 SOA[a]

compounds	average O/C	average H/C	average DBE	average C atoms
group 1 irradiated/fresh > 10	0.48 ± 0.27	1.39 ± 0.86	7.63 ± 2.69	21.76 ± 8.85
group 2 10 > irradiated/fresh > 0.1	0.42 ± 0.22	1.54 ± 0.81	5.55 ± 2.01	19.61 ± 7.32
group 3 irradiated/fresh < 0.1	0.34 ± 0.17	1.60 ± 0.63	7.37 ± 1.89	32.22 ± 8.91
fresh SOA	0.39 ± 0.21	1.57 ± 0.79	5.75 ± 2.00	22.19 ± 7.87
irradiated SOA	0.43 ± 0.31	1.51 ± 0.82	5.82 ± 2.24	19.50 ± 7.48

[a]The Spread in the Observed Values Corresponds to 1σ.

suggesting that they have fewer double bonds per carbon atom. These results are consistent with previous short-term (2 h) photolysis of LIM/O_3 SOA in an aqueous solution and on a filter, in which the O/C ratio increased and the C-number decreased during photolysis.[33]

We calculated the aromaticity index (AI)[58,59] for these molecules, AI = (1 + C − O − 0.5H)/(C−O), and the results show that photodegradation results in the formation/survival of compounds with a larger aromaticity index (Figure 7), although only a small fraction of compounds (<1%) reach the aromaticity index threshold of 0.5 for true aromatic compounds.[58,59] This is also seen in Figure 6b, where photolabile group 3 compounds scatter around the expected DBE vs C asymptote for terpene compounds, while the photorecalcitrant compounds (groups 1 and 2) are closer to the polyenes, suggesting an increase in the number of C═C bonds. All of the observed compounds are below the DBE vs C dependence for the cata-PAHs, ruling out the formation of condensed aromatic products. We should note that enhancement in aromaticity after irradiation has also been observed in dissolved organic matter irradiation studies.[60,61]

Effect of Relative Humidity on Photodegradation. The effect of relative humidity (RH) on photodegradation rates was investigated by flowing air with variable RH over APIN/O_3 and LIM/O_3 SOA during the irradiation (Figure 8). These experiments were limited to early photodegradation times (several hours) because of the difficulties of controlling RH over longer time periods. In both cases, the mass loss increased with increasing RH. Similar effects have been seen in previous photodegradation studies, with mass loss increasing at elevated RH.[13,23,32,65] One of the effects of water vapor is making the SOA matrix less viscous, making it possible for the products of photodegradation to escape more easily from the SOA material. Indeed, the viscosities of α-pinene[66] and D-limonene[65] ozonolysis SOA have been found to decrease with increasing RH. The observation that the mass of dry samples continued to decrease (0% RH traces in Figure 8) even after the LED was switched off supports the idea of slow diffusion of photoproducts out of the SOA matrix. Our results indicate an

https://dx.doi.org/10.1021/acsearthspacechem.0c00088
ACS Earth Space Chem. 2020, 4, 1078−1089

Table 2. List of 10 Molecular Formulas with the Largest Peak Abundances in ESI-MS(+) Spectra in the Fresh LIM/O_3 SOA, Photorecalcitrant (Groups 1 and 2), and Photolabile (Group 3) Groups[a]

fresh SOA formulas	group 1 and 2 formulas	group 3 formulas
$C_{10}H_{16}O_3$	$C_{10}H_{16}O_4$	$C_{20}H_{32}O_5$
$C_{10}H_{16}O_4$	$C_{10}H_{16}O_3$	$C_{29}H_{44}O_8$
$C_{19}H_{30}O_7$	$C_9H_{14}O_4$	$C_{39}H_{62}O_{13}$
$C_{20}H_{32}O_7$	$C_{19}H_{30}O_7$	$C_{39}H_{64}O_{15}$
$C_{19}H_{30}O_8$	$C_{19}H_{30}O_8$	$C_{29}H_{48}O_8$
$C_{19}H_{30}O_6$	$C_{20}H_{32}O_7$	$C_{19}H_{28}O_4$
$C_{20}H_{32}O_8$	$C_{18}H_{28}O_7$	$C_{38}H_{60}O_{12}$
$C_9H_{14}O_4$	$C_{20}H_{32}O_8$	$C_{39}H_{64}O_{14}$
$C_{18}H_{28}O_7$	$C_{12}H_{18}O_5$	$C_{30}H_{48}O_8$
$C_{18}H_{28}O_6$	$C_{19}H_{30}O_6$	$C_{39}H_{64}O_{16}$

[a]The formulas are listed in the order of decreasing normalized peak abundance. Some of the most prominent formulas present in both fresh and irradiated samples may correspond to limonic acid ($C_9H_{14}O_4$), limononic acid ($C_{10}H_{16}O_3$), or 7OH-limononic acid ($C_{10}H_{16}O_4$), as found in previous studies.[62−64]

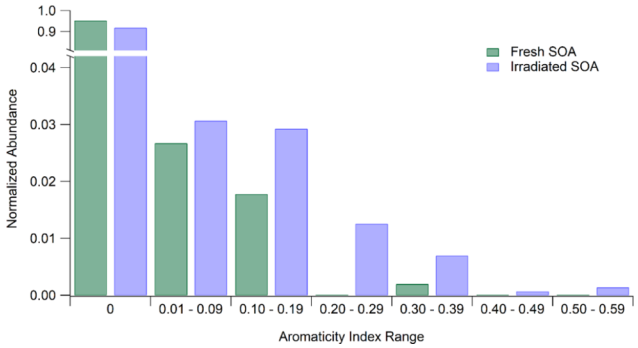

Figure 7. Photodegradation of LIM/O_3 SOA results in the formation/survival of compounds with a larger degree of aromaticity. The histogram shows the normalized abundance of molecules binned into aromaticity index (AI) ranges, where AI > 0.5 corresponds to aromatic compounds.[58,59]

increase in maximum FMLR at ∼60% RH by a factor of 2.3 and 3.1 for APIN/O_3 and LIM/O_3 SOA, respectively (Table S1). These findings agree well with the findings of Wong et al.,[13] who observed an increase of APIN/O_3 SOA mass loss rates by a factor of 2 at high RH conditions compared to dry conditions, and with the result of Arroyo et al.,[32] who reported a 2−4 times higher photodegradation rate for LIM/O_3 SOA at 30−70% RH compared to dry conditions. We should note that at elevated RH, turning the LED off actually resulted in an apparent mass gain. We believe that this is an artifact of the slightly elevated temperature of the QCM crystal under irradiated conditions becoming lower in the darkness, leading to an uptake of water vapor.

Although we attribute the increase in the observed photodegradation rate at higher RH to diffusion transport limitations, we cannot completely rule out the changes in the photochemical mechanism brought about by the presence of water in the SOA material.

Application to Ambient Conditions. To estimate the photodegradation rate of SOA under atmospheric conditions, we assumed that it scales in proportion to the convolution of spectral flux $F(\lambda)$, quantum yield $\phi(\lambda)$, and absorption cross section $\sigma(\lambda)$ (eq 3).

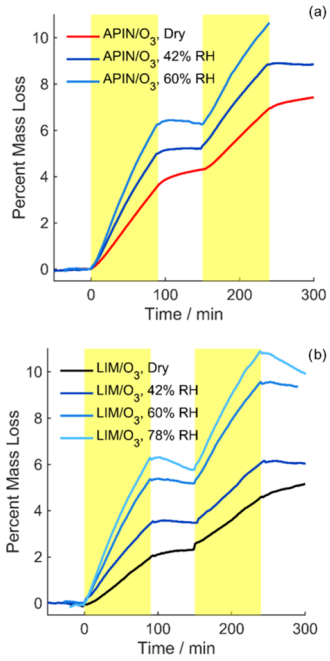

Figure 8. Photodegradation of (a) APIN/O_3 SOA and (b) LIM/O_3 SOA at different relative humidity (RH). The yellow-shaded regions indicate when SOA was being irradiated.

$$\text{FMLR} = -\frac{1}{m}\frac{dm}{dt} = \int F(\lambda)\phi(\lambda)\sigma(\lambda)d\lambda \quad (3)$$

The absorption cross sections and quantum yields of many of these molecules rapidly decay at longer wavelengths,[12,67,68] so the integration can be limited to a narrow range over which the 305 nm LED emits. For a narrow integration range, the ratio of FMLR values for two different radiation sources can be approximated as the ratio of integrated spectral flux densities (eq 4).

$$\text{scaling} = \frac{\int F(\lambda)_{\text{LED}}d\lambda}{\int F(\lambda)_{\text{atm}}d\lambda} \quad (4)$$

The photodegradation profiles were scaled (scaling factor = 1.4) to the 24 h average flux in Los Angeles at the sea level (Figure S4) from the TUV model.[69] This flux corresponded to a 24 h average J_{NO_2} value of 4.05×10^{-3} s^{-1}. The scaled photodegradation rate (Figure 9) shows that the largest mass loss takes place in the first 24 h of exposure, after which the degradation substantially decreases. The scaled percent mass loss profiles of the SOA were fit to a biexponential decay function and are shown in Figure S5 with the intention that they can be utilized by modelers in future studies.

Although photodegradation continues after 24 h, it is substantially slower and other forms of chemical aging, such as heterogeneous oxidation of particles by the hydroxyl radical, may become more important.[29,70] This is highlighted in Figure 10, where the UV degradation mass loss trends are combined with predicted changes as a result of heterogeneous oxidation via OH radicals. We observed that UV degradation dominates in the first 24 h, but heterogeneous OH oxidation becomes increasingly more important after that. It is important to note that the OH aging trend used for this comparison has a few important assumptions:[71] [OH] = 1.5×10^6 molecules cm^{-3}, γ

https://dx.doi.org/10.1021/acsearthspacechem.0c00088
ACS Earth Space Chem. 2020, 4, 1078−1089

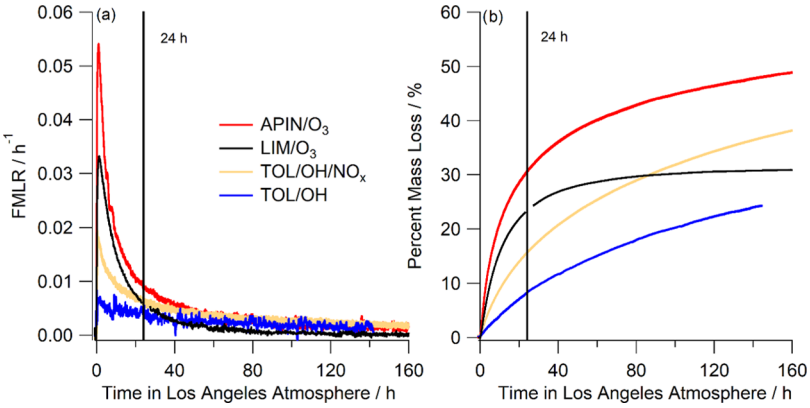

Figure 9. Scaling the results to atmospheric conditions reveals that the FMLR (a) and percent mass loss (b) are most important in the first 24 h of photodegradation. After that, the photodegradation continues at a decreasingly slow rate and other mechanisms of aging become more important.

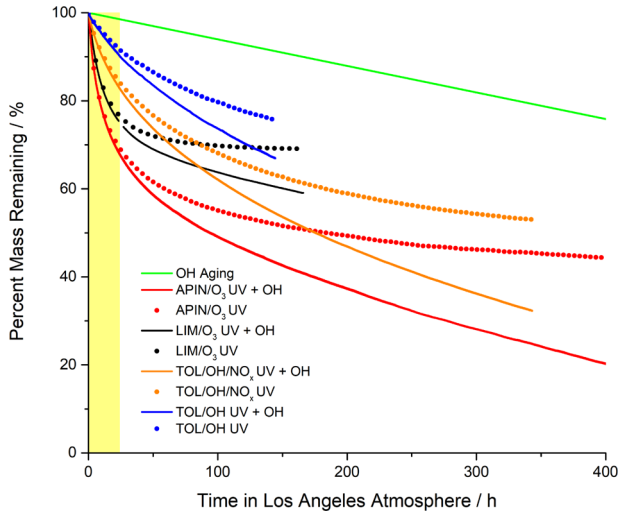

Figure 10. Predicted changes to the percent of mass remaining due to heterogeneous OH aging alone (green line), UV degradation alone (circles), or the combined effect of UV and OH aging (solid curves). The shaded region shows the initial time period where photodegradation is dominant; thereafter, other atmospheric aging mechanisms drive the mass loss.

(uptake coefficient) = 1, average O/C = 0.8, average H/C =1.5, and particle density = 1.5 g cm^{-3}.

The percent of SOA degraded before reaching the photorecalcitrant fraction was also compared to recent studies by O'Brien et al.[29] and Zawadowicz et al.[23] (Figure S6). Overall, our results are similar, especially when comparing the initial photodegradation rate, and all agree on the existence of a photorecalcitrant fraction. Despite the different methods of SOA preparation (flow tube in this study vs a chamber in the other two studies) as well as different irradiation sources used, the measurements agree reasonably well, with a lifetime of 12 h (this study), 7 h (O'Brien et al.), and 23 h (Zawadowicz et al.) of APIN/O_3 SOA degradation (under dry conditions) after scaling to the 24 h average Los Angeles flux. We do however see differences in the photorecalcitrant fraction. This difference may be due to differences in SOA preparation, with a higher mass loading used in this study, which would increase particle-phase partitioning of photoreactive carbonyl group-containing species.

SUMMARY AND IMPLICATIONS

These results have several important implications. First, the mass loss rates observed here are atmospherically relevant. The photodegradation with 254 nm photons showed a maximum FMLR as high as 35% h^{-1} and a complete destruction of the SOA material, proving that SOA can fully degrade under harsh UV radiation. The tropospheric UV irradiation also showed substantial photodegradation, with FMLR up to 5% h^{-1}, and almost half the SOA mass eventually being lost. Thus, SOA photodegradation is an important and substantial component of aging in the atmosphere, especially in the first 24 h after the initial SOA formation, and is crucial to incorporate into models in order to fully understand the effect SOA has on climate and visibility through light absorption/scattering and cloud formation.[23] Overall, while these mass loss rates cannot compete with particle growth for ultrafine particles, which can exceed 10 nm/h,[72] these photodegradation processes can limit the growth of larger particles in the accumulation mode, which dominate the overall SOA mass loading in the atmosphere.[68]

Second, these photodegradation processes should be able to efficiently deplete organic aerosols from the upper troposphere/lower stratosphere after deep convective transport.[73] While we have not done explicit measurements at low temperatures, it can be argued that photodegradation should become relatively more important as the aerosol's viscosity increases at these cool temperatures,[74] thus slowing diffusion in the particle and limiting aging by heterogeneous oxidants like OH radicals. Photodegradation can still occur in these situations because UV radiation can easily penetrate the entire volume of the particle, regardless of its viscosity.

Third, tropospheric photodegradation leads to a photorecalcitrant fraction of SOA remaining, which should be considered when discussing the role of photodegradation in SOA sinks in the atmosphere. Extrapolating the initial mass loss rates and degradation processes to longer time scales would be incorrect and would lead to an overestimate of mass loss, as suggested by O'Brien et al. and Zawadowicz et al.[23,29] Furthermore, the compounds found in the photorecalcitrant fraction are chemically different from those in the initial SOA. More research is needed to better understand the chemical and physical properties of the photorecalcitrant fraction, such as its viscosity and morphology.

And finally, we find that elevated relative humidity increases the mass loss of SOA during photodegradation by acting as a

https://dx.doi.org/10.1021/acsearthspacechem.0c00088
ACS Earth Space Chem. 2020, 4, 1078−1089

plasticizer to reduce the diffusion transport limitations of volatile photoproducts and allowing them to more easily escape from particles. Thus, the relative importance of photodegradative aging vs heterogeneous oxidative aging may shift depending on the environmental conditions, with photodegradation becoming more important in areas with higher relative humidity.

■ ASSOCIATED CONTENT

Supporting Information

The Supporting Information is available free of charge at https://pubs.acs.org/doi/10.1021/acsearthspacechem.0c00088.

It contains a tabular summary of all QCM experiments, description of the method for correction for evaporation, more detailed information about the control experiments, description of the TUV model parameters, and a comparison with the results of O'Brien et al. and Zawadowicz et al. (PDF)

■ AUTHOR INFORMATION

Corresponding Author

Sergey A. Nizkorodov − *Department of Chemistry, University of California, Irvine, California 92697, United States;* orcid.org/0000-0003-0891-0052; Email: nizkorod@uci.edu

Authors

Vahe J. Baboomian − *Department of Chemistry, University of California, Irvine, California 92697, United States;* orcid.org/0000-0002-7274-7109

Yiran Gu − *Department of Chemistry, University of California, Irvine, California 92697, United States*

Complete contact information is available at: https://pubs.acs.org/10.1021/acsearthspacechem.0c00088

Author Contributions

The experiments and data analysis were conceived by S.A.N. and V.J.B. and carried out by Y.G. and V.J.B. The manuscript was written through the contributions of all three co-authors. All authors have given approval to the final version of the manuscript.

Notes

The authors declare no competing financial interest.

■ ACKNOWLEDGMENTS

The authors acknowledge the support from US NSF grant AGS-1853639. The mass spectrometer instrument used in this work was purchased with grant NSF CHE-1920242. V.J.B. thanks the NSF GRFP program for his graduate fellowship. Y.G. thanks the University of California, Irvine Undergraduate Research Opportunities Program for support.

■ REFERENCES

(1) Sindelarova, K.; Granier, C.; Bouarar, I.; Guenther, A.; Tilmes, S.; Stavrakou, T.; Müller, J. F.; Kuhn, U.; Stefani, P.; Knorr, W. Global Data Set of Biogenic VOC Emissions Calculated by the MEGAN Model over the Last 30 Years. *Atmos. Chem. Phys.* **2014**, *14*, 9317−9341.

(2) Kroll, J. H.; Seinfeld, J. H. Chemistry of Secondary Organic Aerosol: Formation and Evolution of Low-Volatility Organics in the Atmosphere. *Atmos. Environ.* **2008**, *42*, 3593−3624.

(3) Hallquist, M.; Wenger, J. C.; Baltensperger, U.; Rudich, Y.; Simpson, D.; Claeys, M.; Dommen, J.; Donahue, N. M.; George, C.; Goldstein, A. H.; Hamilton, J. F.; Herrmann, H.; Hoffmann, T.; Iinuma, Y.; Jang, M.; Jenkin, M. E.; Jimenez, J. L.; Kiendler-Scharr, A.; Maenhaut, W.; McFiggans, G.; Mentel, T. F.; Monod, A.; Prévôt, A. S. H.; Seinfeld, J. H.; Surratt, J. D.; Szmigielski, R.; Wildt, J. The Formation, Properties and Impact of Secondary Organic Aerosol: Current and Emerging Issues. *Atmos. Chem. Phys.* **2009**, *9*, 5155−5236.

(4) Mellouki, A.; Wallington, T. J.; Chen, J. Atmospheric Chemistry of Oxygenated Volatile Organic Compounds: Impacts on Air Quality and Climate. *Chem. Rev.* **2015**, *115*, 3984−4014.

(5) Shrivastava, M.; Cappa, C. D.; Fan, J.; Goldstein, A. H.; Guenther, A. B.; Jimenez, J. L.; Kuang, C.; Laskin, A.; Martin, S. T.; Ng, N. L.; Petaja, T.; Pierce, J. R.; Rasch, P. J.; Roldin, P.; Seinfeld, J. H.; Shilling, J.; Smith, J. N.; Thornton, J. A.; Volkamer, R.; Wang, J.; Worsnop, D. R.; Zaveri, R. A.; Zelenyuk, A.; Zhang, Q. Recent Advances in Understanding Secondary Organic Aerosol: Implications for Global Climate Forcing. *Rev. Geophys.* **2017**, *55*, 509−559.

(6) Moise, T.; Flores, J. M.; Rudich, Y. Optical Properties of Secondary Organic Aerosols and Their Changes by Chemical Processes. *Chem. Rev.* **2015**, *115*, 4400−4439.

(7) George, C.; Ammann, M.; D'Anna, B.; Donaldson, D. J.; Nizkorodov, S. A. Heterogeneous Photochemistry in the Atmosphere. *Chem. Rev.* **2015**, *115*, 4218−4258.

(8) Rudich, Y.; Donahue, N. M.; Mentel, T. F. Aging of Organic Aerosol: Bridging the Gap Between Laboratory and Field Studies. *Annu. Rev. Phys. Chem.* **2007**, *58*, 321−352.

(9) Donahue, N. M.; Robinson, A. L.; Trump, E. R.; Riipinen, I.; Kroll, J. H. Volatility and Aging of Atmospheric Organic Aerosol. In *Atmospheric and Aerosol Chemistry*; Springer: Berlin, Heidelberg, 2012; Vol. *339*, pp 97−143.

(10) Epstein, S. A.; Blair, S. L.; Nizkorodov, S. A. Direct Photolysis of A-Pinene Ozonolysis Secondary Organic Aerosol: Effect on Particle Mass and Peroxide Content. *Environ. Sci. Technol.* **2014**, *48*, 11251−11258.

(11) Malecha, K. T.; Nizkorodov, S. A. Photodegradation of Secondary Organic Aerosol Particles as a Source of Small, Oxygenated Volatile Organic Compounds. *Environ. Sci. Technol.* **2016**, *50*, 9990−9997.

(12) Malecha, K. T.; Cai, Z.; Nizkorodov, S. A. Photodegradation of Secondary Organic Aerosol Material Quantified with a Quartz Crystal Microbalance. *Environ. Sci. Technol. Lett.* **2018**, *5*, 366−371.

(13) Wong, J. P. S.; Zhou, S.; Abbatt, J. P. D. Changes in Secondary Organic Aerosol Composition and Mass Due to Photolysis: Relative Humidity Dependence. *J. Phys. Chem. A* **2015**, *119*, 4309−4316.

(14) Henry, K. M.; Donahue, N. M. Photochemical Aging of α-Pinene Secondary Organic Aerosol: Effects of OH Radical Sources and Photolysis. *J. Phys. Chem. A* **2012**, *116*, 5932−5940.

(15) Pan, X.; Underwood, J. S.; Xing, J.-H.; Mang, S. A.; Nizkorodov, S. A. Photodegradation of Secondary Organic Aerosol Generated from Limonene Oxidation by Ozone Studied with Chemical Ionization Mass Spectrometry. *Atmos. Chem. Phys.* **2009**, *9*, 3851−3865.

(16) Mang, S. A.; Henricksen, D. K.; Bateman, A. E. P.; Andersen, M. P. S.; Blake, D. R.; Nizkorodov, S. A.; Sulbaek Andersen, M. P.; Blake, D. R.; Nizkorodov, S. A. Contribution of Carbonyl Photochemistry to Aging of Atmospheric Secondary Organic Aerosol. *J. Phys. Chem. A* **2008**, *112*, 8337−8344.

(17) Pilinis, C.; Pandis, S. N.; Seinfeld, J. H. Sensitivity of Direct Climate Forcing by Atmospheric Aerosols to Aerosol Size and Composition. *J. Geophys. Res.* **1995**, *100*, 18739−18754.

(18) Gomez, A. L.; Park, J.; Walser, M. L.; Lin, A.; Nizkorodov, S. A. UV Photodissociation Spectroscopy of Oxidized Undecylenic Acid Films. *J. Phys. Chem. A* **2006**, *110*, 3584−3592.

(19) Walser, M. L.; Park, J.; Gomez, A. L.; Russell, A. R.; Nizkorodov, S. A. Photochemical Aging of Secondary Organic Aerosol Particles Generated from the Oxidation of D-Limonene. *J. Phys. Chem. A* **2007**, *111*, 1907−1913.

(20) Walhout, E. Q.; Yu, H.; Thrasher, C.; Shusterman, J. M.; O'Brien, R. E. Effects of Photolysis on the Chemical and Optical Properties of Secondary Organic Material Over Extended Time Scales. *ACS Earth Space Chem.* **2019**, *3*, 1226−1236.
(21) Kamboures, M. A.; Nizkorodov, S. A.; Gerber, R. B. Ultrafast Photochemistry of Methyl Hydroperoxide on Ice Particles. *Proc. Natl. Acad. Sci. U.S.A.* **2010**, *107*, 6600−6604.
(22) Hodzic, A.; Madronich, S.; Kasibhatla, P. S.; Tyndall, G.; Aumont, B.; Jimenez, J. L.; Lee-Taylor, J.; Orlando, J. Organic Photolysis Reactions in Tropospheric Aerosols: Effect on Secondary Organic Aerosol Formation and Lifetime. *Atmos. Chem. Phys.* **2015**, *15*, 9253−9269.
(23) Zawadowicz, M. A.; Lee, B. H.; Shrivastava, M.; Zelenyuk, A.; Zaveri, R. A.; Flynn, C.; Thornton, J. A.; Shilling, J. E. Photolysis Controls Atmospheric Budgets of Biogenic Secondary Organic Aerosol. *Environ. Sci. Technol.* **2020**, *54*, 3861−3870.
(24) Balkanski, Y. J.; Jacob, D. J.; Gardner, G. M.; Graustein, W. C.; Turekian, K. K. Transport and Residence Times of Tropospheric Aerosols Inferred from a Global Three-Dimensional Simulation of 210 Pb. *J. Geophys. Res.* **1993**, *98*, No. 2456.
(25) Heald, C. L.; Coe, H.; Jimenez, J. L.; Weber, R. J.; Bahreini, R.; Middlebrook, A. M.; Russell, L. M.; Jolleys, M.; Fu, T. M.; Allan, J. D.; Bower, K. N.; Capes, G.; Crosier, J.; Morgan, W. T.; Robinson, N. H.; Williams, P. I.; Cubison, M. J.; Decarlo, P. F.; Dunlea, E. J. Exploring the Vertical Profile of Atmospheric Organic Aerosol: Comparing 17 Aircraft Field Campaigns with a Global Model. *Atmos. Chem. Phys.* **2011**, *11*, 12676−12696.
(26) Heald, C. L.; Jacob, D. J.; Park, R. J.; Russell, L. M.; Huebert, B. J.; Seinfeld, J. H.; Liao, H.; Weber, R. J. A Large Organic Aerosol Source in the Free Troposphere Missing from Current Models. *Geophys. Res. Lett.* **2005**, *32*, 1−4.
(27) Bianchi, F.; Tröstl, J.; Junninen, H.; Frege, C.; Henne, S.; Hoyle, C. R.; Molteni, U.; Herrmann, E.; Adamov, A.; Bukowiecki, N.; Chen, X.; Duplissy, J.; Gysel, M.; Hutterli, M.; Kangasluoma, J.; Kontkanen, J.; Kürten, A.; Manninen, H. E.; Münch, S.; Peräkylä, O.; Petäjä, T.; Rondo, L.; Williamson, C.; Weingartner, E.; Curtius, J.; Worsnop, D. R.; Kulmala, M.; Dommen, J.; Baltensperger, U. New Particle Formation in the Free Troposphere: A Question of Chemistry and Timing. *Science* **2016**, *352*, 1109−1112.
(28) Hodzic, A.; Kasibhatla, P. S.; Jo, D. S.; Cappa, C. D.; Jimenez, J. L.; Madronich, S.; Park, R. J. Rethinking the Global Secondary Organic Aerosol (SOA) Budget: Stronger Production, Faster Removal, Shorter Lifetime. *Atmos. Chem. Phys.* **2016**, *16*, 7917−7941.
(29) O'Brien, R. E.; Kroll, J. H. Photolytic Aging of Secondary Organic Aerosol: Evidence for a Substantial Photo-Recalcitrant Fraction. *J. Phys. Chem. Lett.* **2019**, *10*, 4003−4009.
(30) Hung, H. M.; Chen, Y. Q.; Martin, S. T. Reactive Aging of Films of Secondary Organic Material Studied by Infrared Spectroscopy. *J. Phys. Chem. A* **2013**, *117*, 108−116.
(31) Fleming, L. T.; Lin, P.; Roberts, J. M.; Selimovic, V.; Yokelson, R.; Laskin, J.; Laskin, A.; Nizkorodov, S. A. Molecular Composition and Photochemical Lifetimes of Brown Carbon Chromophores in Biomass Burning Organic Aerosol. *Atmos. Chem. Phys.* **2020**, *20*, 1105−1129.
(32) Arroyo, P. C.; Malecha, K. T.; Ammann, M.; Nizkorodov, S. A. Influence of Humidity and Iron(Iii) on Photodegradation of Atmospheric Secondary Organic Aerosol Particles. *Phys. Chem. Chem. Phys.* **2018**, *20*, 30021−30031.
(33) Bateman, A. P.; Nizkorodov, S. A.; Laskin, J.; Laskin, A. Photolytic Processing of Secondary Organic Aerosols Dissolved in Cloud Droplets. *Phys. Chem. Chem. Phys.* **2011**, *13*, 12199.
(34) Nguyen, T. B.; Laskin, A.; Laskin, J.; Nizkorodov, S. A. Direct Aqueous Photochemistry of Isoprene High-NO x Secondary Organic Aerosol. *Phys. Chem. Chem. Phys.* **2012**, *14*, 9702−9714.
(35) Romonosky, D. E.; Li, Y.; Shiraiwa, M.; Laskin, A.; Laskin, J.; Nizkorodov, S. A. Aqueous Photochemistry of Secondary Organic Aerosol of α-Pinene and α-Humulene Oxidized with Ozone, Hydroxyl Radical, and Nitrate Radical. *J. Phys. Chem. A* **2017**, *121*, 1298−1309.
(36) Klodt, A. L.; Romonosky, D. E.; Lin, P.; Laskin, J.; Laskin, A.; Nizkorodov, S. A. Aqueous Photochemistry of Secondary Organic Aerosol of α-Pinene and α-Humulene in the Presence of Hydrogen Peroxide or Inorganic Salts. *ACS Earth Space Chem.* **2019**, *3*, 2736−2746.
(37) Wong, J. P. S.; Tsagkaraki, M.; Tsiodra, I.; Mihalopoulos, N.; Violaki, K.; Kanakidou, M.; Sciare, J.; Nenes, A.; Weber, R. J. Atmospheric Evolution of Molecular-Weight-Separated Brown Carbon from Biomass Burning. *Atmos. Chem. Phys.* **2019**, *19*, 7319−7334.
(38) Aiona, P. K.; Luek, J. L.; Timko, S. A.; Powers, L. C.; Gonsior, M.; Nizkorodov, S. A. Effect of Photolysis on Absorption and Fluorescence Spectra of Light-Absorbing Secondary Organic Aerosols. *ACS Earth Space Chem.* **2018**, *2*, 235−245.
(39) Kroll, J. H.; Lim, C. Y.; Kessler, S. H.; Wilson, K. R. Heterogeneous Oxidation of Atmospheric Organic Aerosol: Kinetics of Changes to the Amount and Oxidation State of Particle-Phase Organic Carbon. *J. Phys. Chem. A* **2015**, *119*, 10767−10783.
(40) Veghte, D. P.; China, S.; Weis, J.; Lin, P.; Hinks, M. L.; Kovarik, L.; Nizkorodov, S. A.; Gilles, M. K.; Laskin, A. Heating-Induced Transformations of Atmospheric Particles: Environmental Transmission Electron Microscopy Study. *Anal. Chem.* **2018**, *90*, 9761−9768.
(41) Hinks, M. L.; Montoya-Aguilera, J.; Ellison, L.; Lin, P.; Laskin, A.; Laskin, J.; Shiraiwa, M.; Dabdub, D.; Nizkorodov, S. A. Effect of Relative Humidity on the Composition of Secondary Organic Aerosol from the Oxidation of Toluene. *Atmos. Chem. Phys.* **2018**, *18*, 1643−1652.
(42) Chen, X.; Hopke, P. K.; Carter, W. P. L. Secondary Organic Aerosol from Ozonolysis of Biogenic Volatile Organic Compounds: Chamber Studies of Particle and Reactive Oxygen Species Formation. *Environ. Sci. Technol.* **2011**, *45*, 276−282.
(43) Krapf, M.; El Haddad, I.; Bruns, E. A.; Molteni, U.; Daellenbach, K. R.; Prévôt, A. S. H.; Baltensperger, U.; Dommen, J. Labile Peroxides in Secondary Organic Aerosol. *Chem* **2016**, *1*, 603−616.
(44) Malecha, K. T.; Nizkorodov, S. A. Feasibility of Photosensitized Reactions with Secondary Organic Aerosol Particles in the Presence of Volatile Organic Compounds. *J. Phys. Chem. A* **2017**, *121*, 4961−4967.
(45) Sauerbrey, G. Verwendung von Schwingquarzen Zur Wägung Dünner Schichten Und Zur Mikrowägung. *Z. Phys.* **1959**, *155*, 206−222.
(46) Wentworth, G. R.; Al-Abadleh, H. A. DRIFTS Studies on the Photosensitized Transformation of Gallic Acid by Iron(Iii) Chloride as a Model for HULIS in Atmospheric Aerosols. *Phys. Chem. Chem. Phys.* **2011**, *13*, 6507−6516.
(47) Romonosky, D. E.; Ali, N. N.; Saiduddin, M. N.; Wu, M.; Lee, H. J. J.; Aiona, P. K.; Nizkorodov, S. A. Effective Absorption Cross Sections and Photolysis Rates of Anthropogenic and Biogenic Secondary Organic Aerosols. *Atmos. Environ.* **2016**, *130*, 172−179.
(48) Liu, J.; Lin, P.; Laskin, A.; Laskin, J.; Kathmann, S. M.; Wise, M.; Caylor, R.; Imholt, F.; Selimovic, V.; Shilling, J. E. Optical Properties and Aging of Light-Absorbing Secondary Organic Aerosol. *Atmos. Chem. Phys.* **2016**, *16*, 12815−12827.
(49) Camredon, M.; Hamilton, J. F.; Alam, M. S.; Wyche, K. P.; Carr, T.; White, I. R.; Monks, P. S.; Rickard, A. R.; Bloss, W. J. Distribution of Gaseous and Particulate Organic Composition during Dark & Alpha-Pinene Ozonolysis. *Atmos. Chem. Phys.* **2010**, *10*, 2893−2917.
(50) Meusinger, C.; Dusek, U.; King, S. M.; Holzinger, R.; Rosenørn, T.; Sperlich, P.; Julien, M.; Remaud, G. S.; Bilde, M.; Röckmann, T.; Johnson, M. S. Chemical and Isotopic Composition of Secondary Organic Aerosol Generated by α -Pinene Ozonolysis. *Atmos. Chem. Phys.* **2017**, *17*, 6373−6391.
(51) Ji, Y.; Zhao, J.; Terazono, H.; Misawa, K.; Levitt, N. P.; Li, Y.; Lin, Y.; Peng, J.; Wang, Y.; Duan, L.; Pan, B.; Zhang, F.; Feng, X.; An, T.; Marrero-Ortiz, W.; Secrest, J.; Zhang, A. L.; Shibuya, K.; Molina,

M. J.; Zhang, R. Reassessing the Atmospheric Oxidation Mechanism of Toluene. *Proc. Natl. Acad. Sci. U.S.A.* **2017**, *114*, 8169−8174.
(52) Lignell, H.; Epstein, S. A.; Marvin, M. R.; Shemesh, D.; Gerber, B.; Nizkorodov, S. Experimental and Theoretical Study of Aqueous Cis-Pinonic Acid Photolysis. *J. Phys. Chem. A* **2013**, *117*, 12930−12945.
(53) Shemesh, D.; Blair, S. L.; Nizkorodov, S. A.; Gerber, R. B. Photochemistry of Aldehyde Clusters: Cross-Molecular versus Unimolecular Reaction Dynamics. *Phys. Chem. Chem. Phys.* **2014**, *16*, 23861−23868.
(54) Epstein, S. A.; Shemesh, D.; Tran, V. T.; Nizkorodov, S. A.; Gerber, R. B. Absorption Spectra and Photolysis of Methyl Peroxide in Liquid and Frozen Water. *J. Phys. Chem. A* **2012**, *116*, 6068−6077.
(55) Barsotti, F.; Bartels-Rausch, T.; De Laurentiis, E.; Ammann, M.; Brigante, M.; Mailhot, G.; Maurino, V.; Minero, C.; Vione, D. Photochemical Formation of Nitrite and Nitrous Acid (HONO) upon Irradiation of Nitrophenols in Aqueous Solution and in Viscous Secondary Organic Aerosol Proxy. *Environ. Sci. Technol.* **2017**, *51*, 7486−7495.
(56) Sangwan, M.; Zhu, L. Absorption Cross Sections of 2-Nitrophenol in the 295−400 Nm Region and Photolysis of 2-Nitrophenol at 308 and 351 Nm. *J. Phys. Chem. A* **2016**, *120*, 9958−9967.
(57) Grygoryeva, K.; Kubečka, J.; Pysanenko, A.; Lengyel, J.; Slavíček, P.; Fárník, M. Photochemistry of Nitrophenol Molecules and Clusters: Intra- vs Intermolecular Hydrogen Bond Dynamics. *J. Phys. Chem. A* **2016**, *120*, 4139−4146.
(58) Koch, B. P.; Dittmar, T. From Mass to Structure: An Aromaticity Index for High-Resolution Mass Data of Natural Organic Matter. *Rapid Commun. Mass Spectrom.* **2016**, *30*, 250.
(59) Koch, B. P.; Dittmar, T. From Mass to Structure: An Aromaticity Index for High-Resolution Mass Data of Natural Organic Matter. *Rapid Commun. Mass Spectrom.* **2006**, *20*, 926−932.
(60) Du, Y.; Zhang, Y.; Chen, F.; Chang, Y.; Liu, Z. Photochemical Reactivities of Dissolved Organic Matter (DOM) in a Sub-Alpine Lake Revealed by EEM-PARAFAC: An Insight into the Fate of Allochthonous DOM in Alpine Lakes Affected by Climate Change. *Sci. Total Environ.* **2016**, *568*, 216−225.
(61) Zhang, Y.; Liu, X.; Osburn, C. L.; Wang, M.; Qin, B.; Zhou, Y. Photobleaching Response of Different Sources of Chromophoric Dissolved Organic Matter Exposed to Natural Solar Radiation Using Absorption and Excitation-Emission Matrix Spectra. *PLoS One* **2013**, *8*, No. e77515.
(62) Walser, M. L.; Desyaterik, Y.; Laskin, J.; Laskin, A.; Nizkorodov, S. A. High-Resolution Mass Spectrometric Analysis of Secondary Organic Aerosol Produced by Ozonation of Limonene. *Phys. Chem. Chem. Phys.* **2008**, *10*, 1009−1022.
(63) Kundu, S.; Fisseha, R.; Putman, A. L.; Rahn, T. A.; Mazzoleni, L. R. Atmospheric Chemistry and Physics High Molecular Weight SOA Formation during Limonene Ozonolysis: Insights from Ultra-high-Resolution FT-ICR Mass Spectrometry Characterization. *Atmos. Chem. Phys* **2012**, *12*, 5523−5536.
(64) Bateman, A. P.; Nizkorodov, S. A.; Laskin, J.; Laskin, A. Time-Resolved Molecular Characterization of Limonene/Ozone Aerosol Using High-Resolution Electrospray Ionization Mass Spectrometry. *Phys. Chem. Chem. Phys.* **2009**, *11*, 7931−7942.
(65) Hinks, M. L.; Brady, M. V.; Lignell, H.; Song, M.; Grayson, J. W.; Bertram, A. K.; Lin, P.; Laskin, A.; Laskin, J.; Nizkorodov, S. A. Effect of Viscosity on Photodegradation Rates in Complex Secondary Organic Aerosol Materials. *Phys. Chem. Chem. Phys.* **2016**, *18*, 8785−8793.
(66) Renbaum-Wolff, L.; Grayson, J. W.; Bateman, A. P.; Kuwata, M.; Sellier, M.; Murray, B. J.; Shilling, J. E.; Martin, S. T.; Bertram, A. K. Viscosity of α-Pinene Secondary Organic Material and Implications for Particle Growth and Reactivity. *Proc. Natl. Acad. Sci. U.S.A.* **2013**, *110*, 8014−8019.
(67) Fagnoni, M. Modern Molecular Photochemistry of Organic Molecules. By Nicholas J. Turro, V. Ramamurthy and Juan C. Scaiano. *Angew. Chem., Int. Ed.* **2010**, *49*, 6709−6710.
(68) Finlayson-Pitts, B. J.; Pitts, J. N. *Chemistry of the Upper and Lower Atmosphere: Theory, Experiments, and Applications*, 1st ed.; Academic Press: San Diego, CA, 2000.
(69) Atmospheric Chemistry Observations & Modeling division/NCAR. Tropospheric Ultraviolet and Visible (TUV) Radiation Model, 2020. https://www2.acom.ucar.edu/modeling/tropospheric-ultraviolet-and-visible-tuv-radiation-model.
(70) George, I. J.; Slowik, J.; Abbatt, J. P. D. Chemical Aging of Ambient Organic Aerosol from Heterogeneous Reaction with Hydroxyl Radicals. *Geophys. Res. Lett.* **2008**, *35*, No. L13811.
(71) Kroll, J. H.; Lim, C. Y.; Kessler, S. H.; Wilson, K. R. Heterogeneous Oxidation of Atmospheric Organic Aerosol: Kinetics of Changes to the Amount and Oxidation State of Particle-Phase Organic Carbon. *J. Phys. Chem. A* **2015**, *119*, 10767−10783.
(72) Smith, J. N.; Dunn, M. J.; VanReken, T. M.; Iida, K.; Stolzenburg, M. R.; McMurry, P. H.; Huey, L. G. Chemical Composition of Atmospheric Nanoparticles Formed from Nucleation in Tecamac, Mexico: Evidence for an Important Role for Organic Species in Nanoparticle Growth. *Geophys. Res. Lett.* **2008**, *35*, No. L04808.
(73) Yu, P.; Rosenlof, K. H.; Liu, S.; Telg, H.; Thornberry, T. D.; Rollins, A. W.; Portmann, R. W.; Bai, Z.; Ray, E. A.; Duan, Y.; Pan, L. L.; Toon, O. B.; Bian, J.; Gao, R. S. Efficient Transport of Tropospheric Aerosol into the Stratosphere via the Asian Summer Monsoon Anticyclone. *Proc. Natl. Acad. Sci. U.S.A.* **2017**, *114*, 6972−6977.
(74) Shiraiwa, M.; Li, Y.; Tsimpidi, A. P.; Karydis, V. A.; Berkemeier, T.; Pandis, S. N.; Lelieveld, J.; Koop, T.; Pöschl, U. Global Distribution of Particle Phase State in Atmospheric Secondary Organic Aerosols. *Nat. Commun.* **2017**, *8*, No. 1525.

https://dx.doi.org/10.1021/acsearthspacechem.0c00088
ACS Earth Space Chem. 2020, 4, 1078−1089